

# Influence of the dynamically disordered N-terminal tail domain on the amyloid core structure of human Y145Stop prion protein fibrils

- 2 Zhe Qi<sup>1</sup>, Krystyna Surewicz<sup>2</sup>, Witold K. Surewicz<sup>2</sup>, Christopher P. Jaroniec<sup>1\*</sup>
- <sup>1</sup>Department of Chemistry and Biochemistry, The Ohio State University, Columbus, OH, USA
- <sup>2</sup>Department of Physiology and Biophysics, Case Western Reserve University, Cleveland, OH, USA
- 4 \* Correspondence:
- 5 Christopher P. Jaroniec
- 6 jaroniec.1@osu.edu
- 7 Keywords: amyloid, prion, octarepeat, intrinsically disordered region/protein, magic-angle
- 8 spinning (MAS) solid-state NMR

10 Abstract

9

13

14

15

16

17

18

19

20

21

22

23

24

25

11 The Y145Stop mutant of human prion protein (huPrP23-144) is associated with a familial prionopathy

and provides a convenient *in vitro* model for investigating amyloid strains and cross-seeding barriers.

huPrP23-144 fibrils feature a compact and relatively rigid parallel in-register β-sheet amyloid core

spanning ~30 C-terminal amino acid residues (~112-141) and a large ~90-residue dynamically

disordered N-terminal tail domain. Here, we systematically evaluate the influence of this dynamic

domain on the structure adopted by the huPrP23-144 amyloid core region, by investigating using

magic-angle spinning solid-state nuclear magnetic resonance (NMR) spectroscopy a series of fibril

samples formed by huPrP23-144 variants corresponding to deletions of large segments of the N-

terminal tail. We find that deletion of the bulk of the N-terminal tail, up to residue 98, yields amyloid

fibrils with native-like huPrP23-144 core structure. Interestingly, deletion of additional flexible

residues in the stretch 99-106 located outside of the amyloid core yields shorter heterogenous fibrils

with fingerprint NMR spectra that are clearly distinct from those for full-length huPrP23-144,

suggestive of the onset of perturbations to the native structure and degree of molecular ordering for the

core residues. For the deletion variant missing residues 99-106 we show that native huPrP23-144 core

structure can be "restored" by seeding the fibril growth with preformed full-length huPrP23-144 fibrils.

## Introduction

26

27 Most peptide and protein molecules are capable of undergoing conformational conversion from their 28 native state into highly ordered, β-sheet rich amyloid fibrils (Dobson, 1999), and for ~50 human 29 proteins such misfolding and amyloid formation can occur under physiological conditions in vivo 30 leading to development of disease (Chiti and Dobson, 2006). A number of amyloids have been found 31 to contain large dynamically disordered domains flanking the structured fibril core (Heise et al., 2005; 32 Siemer et al., 2006; Loquet et al., 2009; Helmus et al., 2010; Bibow et al., 2011; Li et al., 2012; 33 Raveendra et al., 2013; Frederick et al., 2014; Isas, Langen and Siemer, 2015; Cervantes et al., 2016; 34 Lin et al., 2017; Murray et al., 2017; Caulkins et al., 2018; Dregni et al., 2019; Fonda et al., 2021), and it has been suggested that the presence of these conformationally flexible domains may be of 35 36 pathological or functional significance by stabilizing fibril structures and mediating interactions 37 involving protofilaments (Uversky and Fink, 2004; Chiti and Dobson, 2006; Tompa, 2009; van der 38 Wel, 2017; Siemer, 2020). The detailed characterization of dynamically disordered regions in amyloids 39 (and in other large biomacromolecular assemblies) has generally been pursued by multidimensional 40 magic-angle spinning (MAS) nuclear magnetic resonance (NMR) techniques, which are able to 41 visualize these domains directly in hydrated samples at ambient temperature by using experiments 42 based on scalar coupling mediated polarization transfers (Tycko, 2006; van der Wel, 2017; Jaroniec, 43 2019; Siemer, 2020). 44 The C-terminally truncated Y145Stop prion protein (PrP23-144) variant is associated with a hereditary 45 prionopathy in humans (Ghetti et al., 1996), and mouse PrP23-144 amyloid fibrils have recently been 46 shown to cause transmissible prior disease in mice (Choi et al., 2016). Importantly, the highly 47 homologous human (hu), mouse (mo) and Syrian hamster (Sha) PrP23-144 proteins (pairwise amino 48 acid, aa, sequence identities of ~90-95%) have also been shown to provide a valuable in vitro model 49 for detailed investigation of the structural basis of amyloid strains and transmissibility barriers (Kundu 50 et al., 2003; Vanik, Surewicz and Surewicz, 2004; Jones and Surewicz, 2005; Surewicz, Jones and 51 Apetri, 2006). Our previous structural and dynamic solid-state NMR studies of huPrP23-144 fibrils 52 revealed the presence of a structured  $\sim$ 30-residue parallel in-register  $\beta$ -amyloid core (aa  $\sim$ 112-141) 53 exhibiting limited protein backbone motions on the ~0.1-1 ms time scale located near the C-terminus 54 and a large dynamically disordered ~90-residue N-terminal tail domain (aa ~23-110) (Helmus et al., 2008, 2010, 2011; Theint et al., 2018; Aucoin et al., 2019; Shannon et al., 2019). Additional studies of 55 PrP23-144 amyloids containing mutations and deletions corresponding to different huPrP23-144 core 56 57 residues enabled these sequence modifications to be correlated with structural and dynamic changes in

- 58 the PrP23-144 amyloid core and provided initial insights into mammalian PrP23-144 cross-seeding
- 59 specificities (Jones et al., 2011; Theint, Nadaud, Aucoin, et al., 2017; Theint, Nadaud, Surewicz, et al.,
- 60 2017; Dao et al., 2021).
- Previous studies of amyloids formed by full-length prion protein (PrP23-231) and the proteinase-K
- 62 resistant 90-231 fragment of transmissible spongiform encephalopathy associated mammalian PrP
- 63 deposits (Prusiner, 1998) suggest that the flexible N-terminal domain may play a role in PrP
- aggregation properties, and prion structure and pathogenesis (Weissmann, 1999; Lawson et al., 2004;
- Baskakov and Bocharova, 2005; Frankenfield, Powers and Kelly, 2005). The present study aims to
- assess the influence of the dynamic huPrP23-144 N-terminal region on amyloid assembly and resulting
- 67 β-core conformation. This is achieved by performing systematic solid-state NMR, atomic force
- 68 microscopy (AFM) and thioflavin T (ThT) fluorescence studies on fibril samples formed *in vitro* from
- recombinant huPrP23-144 variants corresponding to deletions of large segments of the N-terminal tail.
- Overall, we find that the majority of dynamically disordered N-terminal tail residues, including the
- octarepeat region (aa 51-91) implicated in copper binding and homeostasis (Millhauser, 2007; Aguzzi,
- Baumann and Bremer, 2008), have little impact on the fibril assembly kinetics and ability of the
- deletion variants to adopt the native huPrP23-144 amyloid core structure. However, we also find that
- a stretch of ~10 conformationally flexible residues that precede the amyloid core region in huPrP23-
- 75 144 fibrils appears to play a role in the ability to adopt the native core structure and the degree of
- 76 molecular ordering within the core.

#### Results

- 78 Previous solid-state NMR studies indicate that the relatively rigid β-core region of huPrP23-144 fibrils
- 79 consists of residues 112-141 (Helmus et al., 2008, 2010, 2011; Shannon et al., 2019). In contrast
- 80 residues 23-111 and 142-144 are not observable in conventional cross-polarization magic angle
- spinning (CP-MAS) solid-state NMR spectra that utilize dipolar coupling-based polarization transfers,
- consistent with their increased mobility (van der Wel, 2017; Siemer, 2020) while most of these residues
- 83 can be detected in MAS NMR spectra utilizing polarization transfers mediated via J-couplings (van
- der Wel, 2017; Siemer, 2020). To assess the potential influence of the dynamically disordered N-
- 85 terminal domain of huPrP23-144 on the conformation adopted by the amyloid core region we generated
- a series of fibril samples from large N-terminal domain deletion variants of huPrP23-144 and examined
- 87 their fibrillization kinetics, morphologies and molecular conformations by using ThT fluorescence,
- 88 AFM and solid-state NMR, respectively.

89 The huPrP23-144 deletion variants employed in these studies spanned residues 28-106 – note that the 90 short segment (aa 23-27) containing multiple lysine and arginine residues (as well as the N-terminal 91 GDSP extension present in our huPrP23-144 construct (Helmus et al., 2008) was not deleted in order 92 to ensure the solubility of the different deletion variants. Initially, we investigated the following 93 huPrP23-144 variants:  $\Delta$ 28-50,  $\Delta$ 51-91 (corresponding to deletion of the entire octarepeat region) and 94  $\Delta$ 92-106 (see Figure 3a for the huPrP23-144 protein sequence and summary of the deletion variants 95 studied). Briefly, fibrils generated from the  $\Delta 28$ -50 and  $\Delta 51$ -91 constructs were found to exhibit wild-96 type (WT) like morphologies and molecular conformations, while significant differences relative to 97 WT were observed for the  $\Delta 92$ -106 fibrils. To investigate this further we prepared the  $\Delta 92$ -98 variant, 98 which was found to form WT-like fibrils suggesting that deletion of huPrP23-144 N-terminal residues 99 up to aa 98 does not have a significant impact on formation of the native huPrP23-144 amyloid core 100 structure. Based on these findings we then generated the  $\Delta 28$ -98 variant corresponding to the deletion 101 of nearly the entire huPrP23-144 N-terminal tail. While the  $\Delta$ 28-98 construct expressed at reasonable 102 level in rich medium it was found not to express at sufficiently high level in <sup>13</sup>C and <sup>15</sup>N isotope 103 enriched minimal medium to permit multidimensional solid-state NMR studies, which led us to 104 generate an additional,  $\Delta 28-91$ , deletion variant. The studies of all the aforementioned huPrP23-144 105 N-terminal deletion variants are described in additional detail below.

106 As noted above, all the huPrP23-144 deletion variants investigated in this study ( $\Delta 28-50$ ,  $\Delta 28-91$ ,  $\Delta 28-1$ ,  $\Delta 28$ 107 98,  $\Delta$ 51-91,  $\Delta$ 92-98 and  $\Delta$ 92-106) readily converted to amyloid fibrils in autocatalytic, unseeded 108 reactions carried out in potassium phosphate buffer at pH 6.4. The kinetics of fibril formation were 109 monitored by the standard ThT binding assay (Naiki et al., 1989) revealing a nearly identical ~3-4 h 110 lag phase for WT huPrP23-144 and all the deletion variants at 400 µM protein concentration, in line 111 with the value reported previously for WT huPrP23-144 (Kundu et al., 2003). Representative data for 112 WT,  $\Delta 28$ -91 and  $\Delta 92$ -106 huPrP23-144 are shown in Figure 1. Furthermore, we found that addition of 113 a small amount of pre-formed WT huPrP23-144 fibril seeds to the reaction resulted in complete 114 elimination of the lag phase for all deletion variants studied (Figure 1).

Atomic force microscopy was then used to investigate the morphologies of the resulting amyloid fibrils. With exception of the Δ92-106 fibrils, all the other deletion variants displayed morphologies that were similar to one another as well as to the morphology of WT huPrP23-144 amyloid. Specifically, as shown in Figure 2, these fibrils had highly uniform, micron long, threadlike morphologies with left-handed twist characterized by heights of ~5-6 nm and periodicities of ~30 nm.

In contrast, the Δ92-106 fibril sample was far more heterogeneous, containing shorter fibrils of varying
lengths in the range of tens to hundreds of nanometers as well as considerable amounts of apparently
amorphous, non-fibrillar aggregates (Figure 2c).

Finally, in order to compare the protein conformations and degree of molecular ordering for the different fibril samples at the atomic level, we recorded two-dimensional (2D) fingerprint <sup>15</sup>N-<sup>13</sup>Cα chemical shift correlation solid-state NMR spectra for wild-type huPrP23-144 amyloid and all the deletion variants except  $\Delta 28$ -98. Figure 3 shows the resulting 2D  $^{15}$ N- $^{13}$ C $\alpha$  spectra, which were found to be effectively identical in terms of NMR signal frequencies, linewidths and relative intensities for WT huPrP23-144 and all deletion variants with exception of Δ92-106 fibrils; the latter exhibited considerable spectral differences relative to the other samples (Figure 3f). Note that for fibrils formed from the  $\Delta 28$ -98 variant, which did not express at a sufficiently high level in  $^{13}$ C and  $^{15}$ N isotope labeled minimal media to permit collection of a <sup>15</sup>N-<sup>13</sup>Cα correlation spectrum, a 1D <sup>13</sup>C CP-MAS spectrum could be recorded for unlabeled fibrils (Figure 4). Apart from the obviously lower sensitivity associated with the use of a natural abundance sample, this spectrum showed considerable similarity to the reference <sup>13</sup>C CP-MAS spectrum recorded for <sup>13</sup>C, <sup>15</sup>N-labeled WT huPrP23-144 fibrils. Altogether these data indicate that other than Δ92-106, all the huPrP23-144 deletion variants studied form amyloids that are highly ordered at the atomic level and possess WT-like core structures and core residue backbone motions. On the other hand, the spectra of  $\Delta 92$ -106 fibrils are indicative of structural perturbation/polymorphism for the core residues and a higher degree of molecular disorder, consistent with the higher degree of sample heterogeneity observed by AFM. Comparison of 2D  $^{15}$ N- $^{13}$ C $\alpha$  spectra for WT and  $\Delta 92$ -106 fibrils reveals that they key chemical shift perturbations involve residues ~112-115. This suggests that conformations of the \beta1-strand and several following core residues are primarily impacted in the deletion variant, in line with earlier studies (Theint, Nadaud, Aucoin, et al., 2017) indicating that several residues in this regime appear to be key for stabilizing the core fold of WT huPrP23-144 amyloid. Remarkably, however, we also find that seeding Δ92-106 amyloid formation with pre-formed WT huPrP23-144 fibrils results in the structural adaptation of the  $\Delta 92$ -106 protein to the WT huPrP23-144 amyloid core fold as evidenced by their indistinguishable 2D <sup>15</sup>N-<sup>13</sup>Cα spectra (Figure 3g).

148

123

124

125

126

127

128

129

130

131

132

133

134

135

136

137

138

139

140

141

142

143

144

145

146

147

#### Discussion

150

151 Collectively, on the basis of effectively identical fibril assembly kinetics, morphologies and fingerprint 152 solid-state NMR spectra for all huPrP23-144 variants studied containing large deletions up to residue 153 98, our results indicate that the bulk of the dynamically disordered N-terminal tail domain of huPrP23-154 144 is not essential for amyloid formation under autocatalytic conditions and ability of the resulting β-155 core region to adopt a WT-like structure. Remarkably, this finding is strongly correlated with our 156 previously reported data showing that proteinase-K resistant fragments of WT huPrP23-144 amyloid 157 fibrils span residues 97-144, 98-144 and 99-144 (Jones et al., 2011). 158 Combined with the finding that the protein conformation and degree of molecular ordering appear to 159 be significantly perturbed for the  $\Delta 92-106$  deletion variant relative to WT huPrP23-144 and the 160 different large huPrP23-144 deletion variants up to residue 98, our data indicate that aa ~99-106 (and 161 presumably several additional amino acids preceding the structured and relatively rigid fibril core 162 beginning around residue Met-112) play a key role in stabilizing the formation of the characteristic 163 huPrP23-144 β-core structure in spite of their flexible nature and location outside of the structured 164 amyloid core region. Given that the 100-110 stretch of huPrP23-144 contains four positively charged 165 lysine residues (at positions 101, 104, 106 and 110) we speculate that the stabilization of the amyloid 166 core structure in WT huPrP23-144 occurs via electrostatic interactions with the negatively charged C-167 terminal aspartate residue. 168 While deletion of amino acids in the 99-106 regime clearly impacts the amyloid core structure and 169 molecular ordering of huPrP23-144 within fibrils formed under autocatalytic conditions as discussed 170 above, we also find that the seeding of fibril formation by the  $\Delta 92-106$  deletion variant with pre-formed 171 WT huPrP23-144 fibrils at low concentration leads to the Δ92-106 proteins adopting a WT-like core structure at the atomic level as revealed by the fingerprint  $^{15}N$ - $^{13}C\alpha$  NMR spectrum that is effectively 172 173 identical to the corresponding spectrum for WT huPrP23-144 amyloid. Interestingly, this structural 174 templating process that yields a WT-like fold for  $\Delta 92\text{-}106$  amyloid was found to not appreciably alter 175 the overall morphology of the  $\Delta 92-106$  fibrils as viewed by AFM, with the majority of the sample 176 consisting of relatively short fibrils similar to those observed in the unseeded reaction. 177 In summary, we systematically evaluated the influence of the dynamically disordered N-terminal tail 178 domain of huPrP23-144 on the structure adopted by the amyloid core region by using deletion 179 mutagenesis combined with magic-angle spinning solid-state NMR spectroscopy. We find that N-180 terminal huPrP23-144 residues up to aa 98, which coincide with the protein segment most susceptible

to proteinase-K digestion in mature fibrils, can be deleted without impacting the core structure formed 182 in an autocatalytic fibril assembly process. Remarkably, deletion of additional flexible residues (aa 99-183 106) located outside the amyloid core leads to the formation of amyloid fibrils with a perturbed core 184 structure and reduced degree of molecular ordering in the fibril lattice, most likely caused by the disruption of stabilizing electrostatic interactions involving several lysine side-chains found in this region and the C-terminal aspartate residue. These structural perturbations, however, can be alleviated by catalyzing the amyloid formation with preformed WT huPrP23-144 fibril seeds.

188

189

190

191

192

193

194

195

196

185

186

187

181

#### **Materials and Methods**

Protein expression and purification. The plasmid encoding human PrP23-144 was described previously (Kundu et al., 2003) and plasmids encoding huPrP23-144 deletion variants were generated similarly to our previous study (Jones et al., 2011) by deletion mutagenesis using a QuikChange kit (Stratagene). Uniformly <sup>13</sup>C, <sup>15</sup>N labeled huPrP23-144 and deletion variants were expressed in E. coli BL21 (DE3) cells and purified by nickel affinity chromatography as described in detail in previous studies (Theint, Nadaud, Surewicz, et al., 2017; Dao et al., 2021). The identities and purities of the resulting proteins were routinely confirmed by SDS/PAGE and MALDI mass spectrometry.

197

198 Amyloid fibril formation. Amyloid fibrils were prepared under quiescent conditions at 25 °C as 199 described in previous studies (Theint, Nadaud, Aucoin, et al., 2017; Theint, Nadaud, Surewicz, et al., 200 2017; Dao et al., 2021). Lyophilized huPrP23-144 variants were dissolved in ultrapure water at ~400 201 µM concentration and 1 M potassium phosphate buffer at pH 6.4 was added to a final concentration of 202 50 mM. For samples seeded with WT huPrP23-144 amyloid, 2% (mole fraction) of preformed fibrils 203 was added immediately to the reaction after addition of phosphate buffer.

204

205 Thioflavin T fluorescence and atomic force microscopy. Kinetics of fibril formation were monitored 206 via the standard ThT fluorescence assay (Naiki et al., 1989) as described in detail in previous studies 207 (Theint et al., 2018). Fibril morphologies were assessed by atomic force microscopy (AFM) as follows. 208 Fibril suspensions were diluted 50-fold in ultrapure water, deposited on freshly cleaved mica substrates 209 (Ted Pella Inc.) for 5 min, rinsed with three 50 µL aliquots of ultrapure water, and allowed to air dry 210 for 1-2 h prior to imaging. Images were collected using a Bruker Dimension Icon AFM in PeakForce

211	quantitative nanomechanical mapping mode with a ScanAsyst-Air probe and processed with the
212	Bruker NanoScope Analysis software.
213	
214	Solid-state NMR spectroscopy. Fibril suspensions for solid-state NMR analysis were incubated as
215	described above for 48 h and centrifuged. The fibril pellets were washed three times with 50 mM
216	potassium phosphate pH 6.4 buffer and packed into 3.2 mm zirconia rotors by centrifugation with the
217	final samples containing ${\sim}5\text{-}10$ mg of fibrils. Standard 1D $^{13}C$ CP-MAS and 2D $^{15}N\text{-}^{13}C\alpha$ solid-state
218	NMR spectra were recorded on 500 MHz Varian and 800 MHz Bruker spectrometers, equipped with
219	3.2 mm triple resonance ( <sup>1</sup> H- <sup>13</sup> C- <sup>15</sup> N) BioMAS and E <sup>free</sup> probes, respectively. The sample temperature
220	and MAS frequencies were actively regulated at 5 °C and 11.111 kHz, respectively, and the
221	experimental parameters were similar to those used in our previous solid-state NMR studies of WT
222	huPrP23-144 fibrils (Helmus $\it et~al.$ , 2008) with data acquisition times for the 2D $^{15}$ N- $^{13}$ C $\alpha$ NMR spectra
223	of 8-16 h per sample. NMR spectra were processed and analyzed using NMRPipe (Delaglio et al.,
224	1995) and Sparky (Goddard and Kneller, 2006), respectively.
225	
226	Conflict of Interest
227	The authors declare that the research was conducted in the absence of any commercial or financial
228	relationships that could be construed as a potential conflict of interest.
229	<b>Author Contributions</b>
230	WKS and CPJ designed the study. ZQ and KS prepared samples and performed experiments. ZQ
231	prepared figures. ZQ, WKS and CPJ wrote the manuscript.
232	Funding
233	This work was supported by grants from NIH (R01GM094357 to CPJ and WKS and S10OD012303
234	to CPJ) and NSF (MCB-1715174 to CPJ).
235	Acknowledgments
236	We thank Dr. Sean Smrt for stimulating discussions and insightful comments on the manuscript.

#### 237 References

- Aguzzi, A., Baumann, F. and Bremer, J. (2008) The prion's elusive reason for being, *Annu. Rev.*
- 239 *Neurosci.* 31, 439–477. doi: 10.1146/annurev.neuro.31.060407.125620.
- Aucoin, D. et al. (2019) Protein-solvent interfaces in human Y145Stop prion protein amyloid fibrils
- probed by paramagnetic solid-state NMR spectroscopy, J. Struct. Biol. 206(1), 36–42. doi:
- 242 10.1016/j.jsb.2018.04.002.
- 243 Baskakov, I. V and Bocharova, O. V (2005) In vitro conversion of mammalian prion protein into
- amyloid fibrils displays unusual features, *Biochemistry*. 44(7), 2339–2348. doi: 10.1021/bi048322t.
- Bibow, S. et al. (2011) The dynamic structure of filamentous tau, Angew. Chem. Int. Ed. 50(48),
- 246 11520–11524. doi: 10.1002/anie.201105493.
- Caulkins, B. G. et al. (2018) Dynamics of the proline-rich C-Terminus of huntingtin exon-1 fibrils, J.
- 248 *Phys. Chem. B.* 122(41), 9507–9515. doi: 10.1021/acs.jpcb.8b09213.
- 249 Cervantes, S. A. et al. (2016) Identification and structural characterization of the N-terminal amyloid
- 250 core of Orb2 isoform A, Sci. Rep. 6, 38265. doi: 10.1038/srep38265.
- 251 Chiti, F. and Dobson, C. M. (2006) Protein misfolding, functional amyloid, and human disease,
- 252 Annu. Rev. Biochem. 75, 333–366. doi: 10.1146/annurev.biochem.75.101304.123901.
- 253 Choi, J.-K. et al. (2016) Amyloid fibrils from the N-terminal prion protein fragment are infectious,
- 254 Proc. Natl. Acad. Sci. USA 113(48), 13851–13856. doi: 10.1073/pnas.1610716113.
- Dao, H. H. et al. (2021) <sup>13</sup>C and <sup>15</sup>N chemical shift assignments of A117V and M129V human
- 256 Y145Stop prion protein amyloid fibrils, *Biomol. NMR Assign.* 15(1), 45–51. doi: 10.1007/s12104-
- 257 020-09981-4.
- Delaglio, F. et al. (1995) NMRPipe: A multidimensional spectral processing system based on UNIX
- 259 pipes, J. Biomol. NMR, 6(3), 277–293. doi: 10.1007/BF00197809.
- Dobson, C. M. (1999) Protein misfolding, evolution and disease, Trends Biochem. Sci. 24(9), 329-
- 261 332. doi: 10.1016/s0968-0004(99)01445-0.
- Dregni, A. J. et al. (2019) In vitro 0N4R tau fibrils contain a monomorphic β-sheet core enclosed by
- 263 dynamically heterogeneous fuzzy coat segments, *Proc. Natl. Acad. Sci. USA* 116(33), 16357–16366.
- 264 doi: 10.1073/pnas.1906839116.
- Fonda, B. D. et al. (2021) Identification of the rigid core for aged liquid droplets of an RNA-binding
- 266 protein low complexity domain, J. Am. Chem. Soc. 143(17), 6657–6668. doi: 10.1021/jacs.1c02424.
- Frankenfield, K. N., Powers, E. T. and Kelly, J. W. (2005) Influence of the N-terminal domain on the
- 268 aggregation properties of the prion protein, *Prot. Sci.* 14(8), 2154–2166. doi: 10.1110/ps.051434005.
- Frederick, K. K. et al. (2014) Distinct prion strains are defined by amyloid core structure and
- 270 chaperone binding site dynamics, *Chem. Biol.* 21(2), 295–305. doi: 10.1016/j.chembiol.2013.12.013.
- 271 Ghetti, B. et al. (1996) Vascular variant of prion protein cerebral amyloidosis with tau-positive

- 272 neurofibrillary tangles: the phenotype of the stop codon 145 mutation in PRNP, *Proc. Natl. Acad.*
- 273 Sci. USA 93(2), 744–748. doi: 10.1073/pnas.93.2.744.
- Goddard, T. and Kneller, D. (2006) SPARKY 3. San Francisco: University of Califronia.
- Heise, H. et al. (2005) Molecular-level secondary structure, polymorphism, and dynamics of full-
- length alpha-synuclein fibrils studied by solid-state NMR, Proc. Natl. Acad. Sci. USA 102(44),
- 277 15871–15876. doi: 10.1073/pnas.0506109102.
- Helmus, J. J. et al. (2008) Molecular conformation and dynamics of the Y145Stop variant of human
- prion protein in amyloid fibrils, Proc. Natl. Acad. Sci. USA 105(17), 6284–6289. doi:
- 280 10.1073/pnas.0711716105.
- Helmus, J. J. et al. (2010) Conformational flexibility of Y145Stop human prion protein amyloid
- 282 fibrils probed by solid-state nuclear magnetic resonance spectroscopy, J. Am. Chem. Soc. 132(7),
- 283 2393–2403. doi: 10.1021/ja909827v.
- Helmus, J. J. et al. (2011) Intermolecular alignment in Y145Stop human prion protein amyloid fibrils
- probed by solid-state NMR spectroscopy, J. Am. Chem. Soc. 133(35), 13934–13937. doi:
- 286 10.1021/ja206469q.
- Isas, J. M., Langen, R. and Siemer, A. B. (2015) Solid-state nuclear magnetic resonance on the static
- and dynamic domains of huntingtin exon-1 fibrils, *Biochemistry*, 54(25), 3942–3949. doi:
- 289 10.1021/acs.biochem.5b00281.
- Jaroniec, C. P. (2019) Two decades of progress in structural and dynamic studies of amyloids by
- 291 solid-state NMR, *J. Magn. Reson.* 306, 42–47. doi: 10.1016/j.jmr.2019.07.015.
- Jones, E. M. et al. (2011) Structural polymorphism in amyloids: new insights from studies with
- 293 Y145Stop prion protein fibrils, J. Biol. Chem. 286(49), 42777–42784. doi:
- 294 10.1074/jbc.M111.302539.
- Jones, E. M. and Surewicz, W. K. (2005) Fibril conformation as the basis of species- and strain-
- dependent seeding specificity of mammalian prion amyloids, *Cell* 121(1), 63–72. doi:
- 297 10.1016/j.cell.2005.01.034.
- 298 Kundu, B. et al. (2003) Nucleation-dependent conformational conversion of the Y145Stop variant of
- 299 human prion protein: structural clues for prion propagation, *Proc. Natl. Acad. Sci. USA* 100(21),
- 300 12069–12074. doi: 10.1073/pnas.2033281100.
- Lawson, V. A. et al. (2004) Flexible N-terminal region of prion protein influences conformation of
- 302 protease-resistant prion protein isoforms associated with cross-species scrapie infection in vivo and
- 303 in vitro, J. Biol. Chem., 279(14), 13689–13695. doi: 10.1074/jbc.M303697200.
- Li, J. et al. (2012) The RIP1/RIP3 necrosome forms a functional amyloid signaling complex required
- 305 for programmed necrosis, *Cell* 150(2), 339–350. doi: 10.1016/j.cell.2012.06.019.
- Lin, H.-K. et al. (2017) Fibril polymorphism affects immobilized non-amyloid flanking domains of
- huntingtin exon1 rather than its polyglutamine core, *Nat. Comm.* 8, 15462. doi:
- 308 10.1038/ncomms15462.

- Loquet, A. et al. (2009) Prion fibrils of Ure2p assembled under physiological conditions contain
- 310 highly ordered, natively folded modules, J. Mol. Biol. 394(1), 108–118. doi:
- 311 10.1016/j.jmb.2009.09.016.
- 312 Millhauser, G. L. (2007) Copper and the prion protein: methods, structures, function, and disease,
- 313 Annu. Rev. Phys. Chem. 58, 299–320. doi: 10.1146/annurev.physchem.58.032806.104657.
- Murray, D. T. et al. (2017) Structure of FUS protein fibrils and its relevance to self-Assembly and
- 315 phase separation of low-complexity domains, Cell 171(3), 615-627.e16. doi:
- 316 10.1016/j.cell.2017.08.048.
- Naiki, H. et al. (1989) Fluorometric determination of amyloid fibrils in vitro using the fluorescent
- 318 dye, thioflavin T1, *Anal. Biochem.* 177(2), 244–249. doi: 10.1016/0003-2697(89)90046-8.
- 319 Prusiner, S. B. (1998) Prions, *Proc. Natl. Acad. Sci. USA*, 95(23), 13363–13383. doi:
- 320 10.1073/pnas.95.23.13363.
- Raveendra, B. L. et al. (2013) Characterization of prion-like conformational changes of the neuronal
- 322 isoform of Aplysia CPEB, *Nat. Struct. Mol. Biol.* 20(4), 495–501. doi: 10.1038/nsmb.2503.
- 323 Shannon, M. D. et al. (2019) Conformational dynamics in the core of human Y145Stop prion protein
- amyloid probed by relaxation dispersion NMR, ChemPhysChem 20(2), 311–317. doi:
- 325 10.1002/cphc.201800779.
- 326 Siemer, A. B. et al. (2006) Observation of highly flexible residues in amyloid fibrils of the HET-s
- 327 prion, J. Am. Chem. Soc. 128(40), 13224–13228. doi: 10.1021/ja063639x.
- 328 Siemer, A. B. (2020) Advances in studying protein disorder with solid-state NMR, *Solid State Nucl.*
- 329 *Magn. Reson.* 106, 101643. doi: 10.1016/j.ssnmr.2020.101643.
- 330 Surewicz, W. K., Jones, E. M. and Apetri, A. C. (2006) The emerging principles of mammalian prion
- propagation and transmissibility barriers: Insight from studies in vitro, Acc. Chem. Res. 39(9), 654–
- 332 662. doi: 10.1021/ar050226c.
- Theint, T., Nadaud, P. S., Surewicz, K., et al. (2017) <sup>13</sup>C and <sup>15</sup>N chemical shift assignments of
- mammalian Y145Stop prion protein amyloid fibrils, *Biomol. NMR Assign.* 11(1), 75–80. doi:
- 335 10.1007/s12104-016-9723-6.
- Theint, T., Nadaud, P. S., Aucoin, D., et al. (2017) Species-dependent structural polymorphism of
- Y145Stop prion protein amyloid revealed by solid-state NMR spectroscopy, *Nat. Comm.* 8(1), 753.
- 338 doi: 10.1038/s41467-017-00794-z.
- Theint, T. et al. (2018) Structural studies of amyloid fibrils by paramagnetic solid-state nuclear
- magnetic resonance spectroscopy, J. Am. Chem. Soc 140(41), 13161–13166. doi:
- 341 10.1021/jacs.8b06758.
- Tompa, P. (2009) Structural disorder in amyloid fibrils: its implication in dynamic interactions of
- 343 proteins, FEBS J. 276(19), 5406–5415. doi: 10.1111/j.1742-4658.2009.07250.x.
- Tycko, R. (2006) Molecular structure of amyloid fibrils: insights from solid-state NMR, Q. Rev.

345	Biophys. 39(1), 1–55. doi: 10.1017/S0033583506004173.
346 347 348	Uversky, V. N. and Fink, A. L. (2004) Conformational constraints for amyloid fibrillation: The importance of being unfolded, <i>Biochim. Biophys. Acta</i> 1698(2), 131–153. doi: 10.1016/j.bbapap.2003.12.008.
349 350 351	Vanik, D. L., Surewicz, K. A. and Surewicz, W. K. (2004) Molecular basis of barriers for interspecies transmissibility of mammalian prions, <i>Mol. Cell.</i> 14(1), 139–145. doi: 10.1016/s1097-2765(04)00155-8.
352 353	Weissmann, C. (1999) Molecular genetics of transmissible spongiform encephalopathies, <i>J. Biol. Chem.</i> 274(1), 3–6. doi: 10.1074/jbc.274.1.3.
354 355	van der Wel, P. C. A. (2017) Insights into protein misfolding and aggregation enabled by solid-state NMR spectroscopy, <i>Solid State Nucl. Magn. Reson.</i> 88, 1–14. doi: 10.1016/j.ssnmr.2017.10.001.
356	
357	
358	

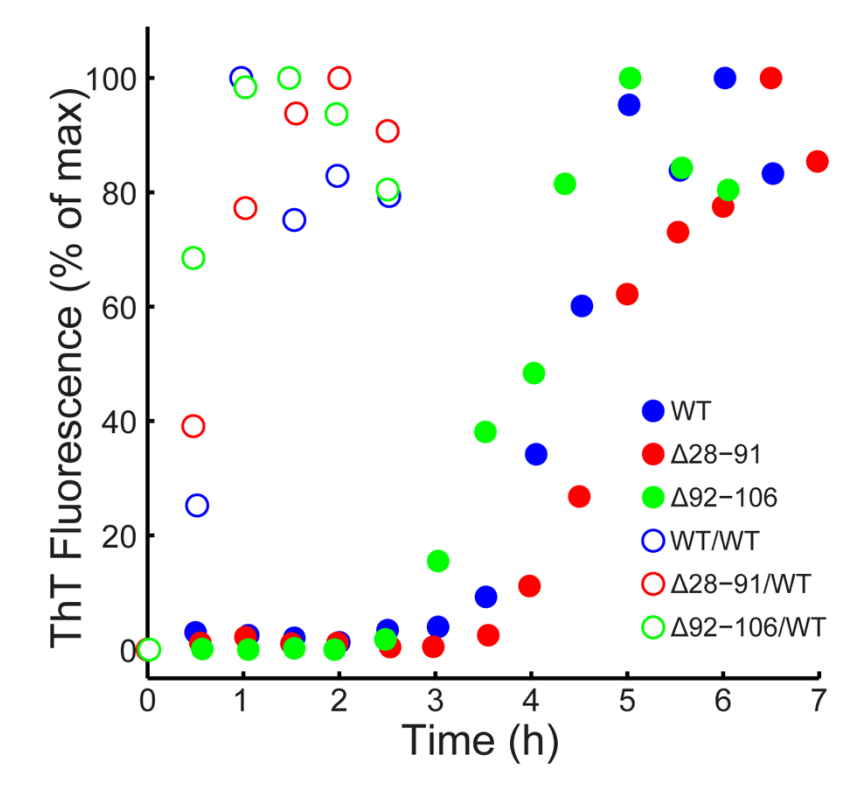


**Figure 1.** Kinetics of amyloid formation monitored by thioflavin T fluorescence in the absence (filled circles) and presence (open circles) of 2% (mole fraction) of WT huPrP23-144 fibril seeds for WT (blue),  $\Delta$ 28-91 (red) and  $\Delta$ 92-106 (green) huPrP23-144.

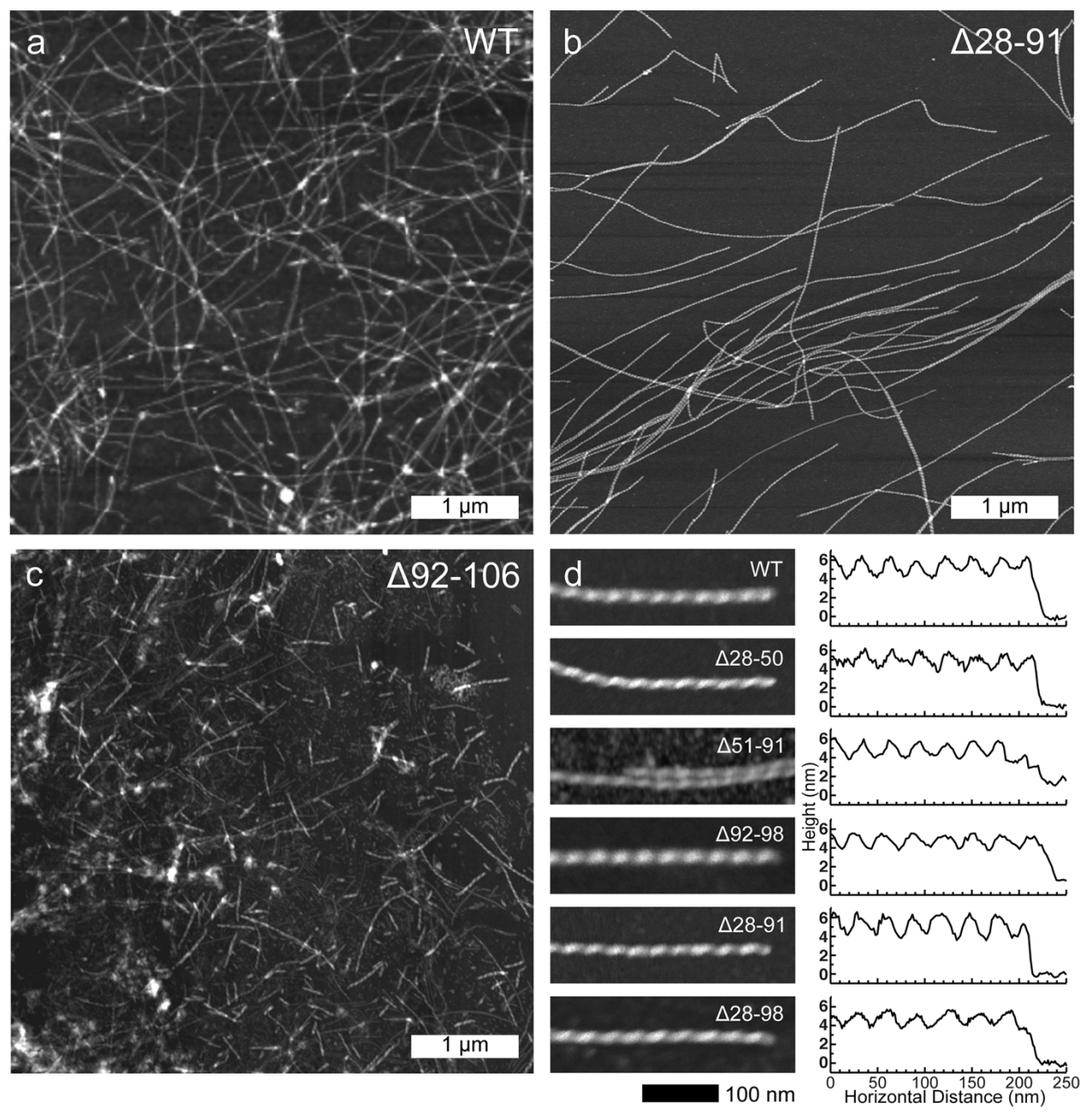


**Figure 2.** Representative low-resolution atomic force microscopy images for (a) WT, (b)  $\Delta 28$ -91 and (c)  $\Delta 92$ -106 huPrP23-144 fibrils (scale bar 1µm for all panels). (d) High-resolution atomic force microscopy images (left; scale bar 100 nm for all panels) and corresponding height profiles (right) for WT,  $\Delta 28$ -50,  $\Delta 51$ -91,  $\Delta 92$ -98,  $\Delta 28$ -91, and  $\Delta 28$ -98 huPrP23-144 fibrils as indicated in the insets.

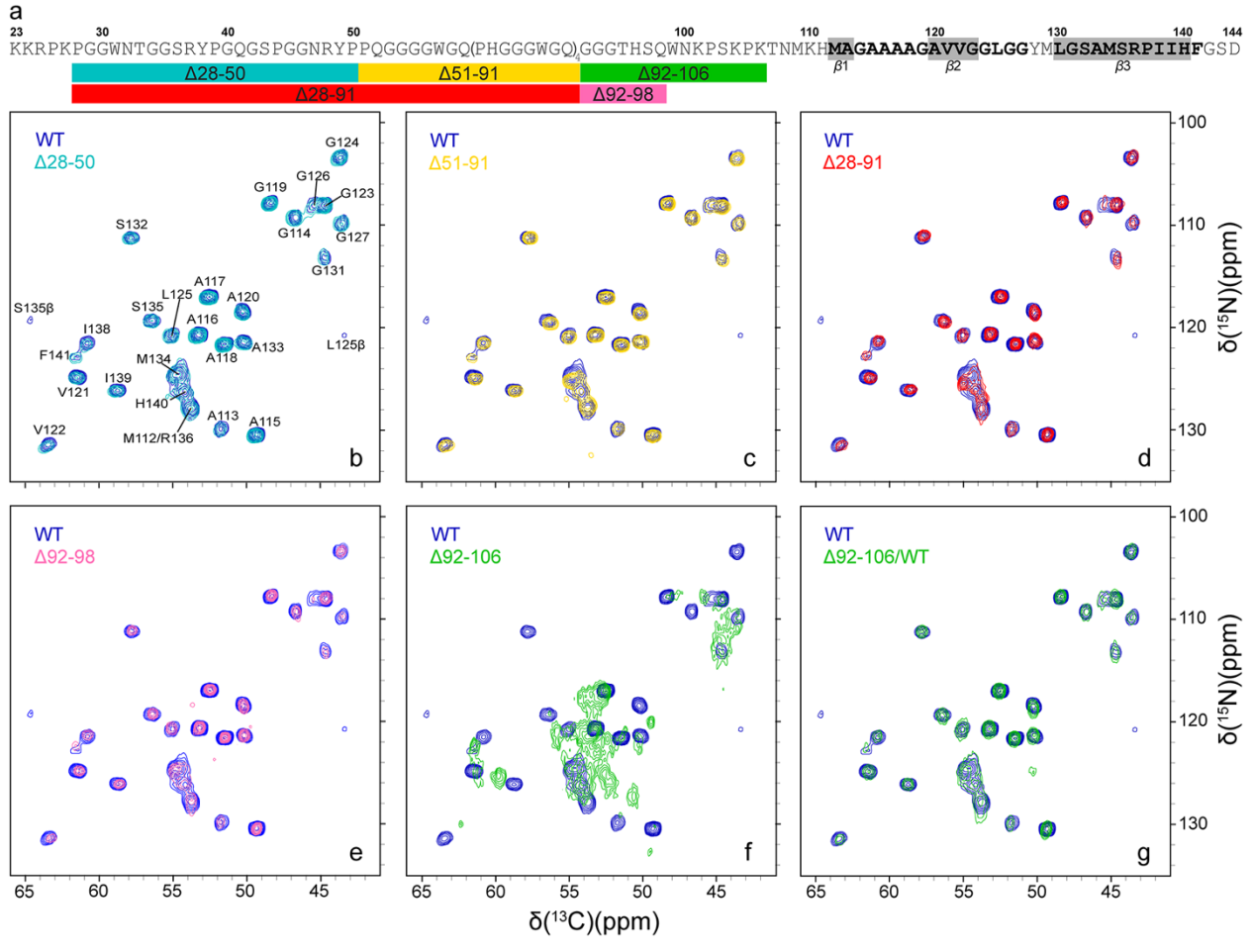


**Figure 3.** (a) Amino acid sequence of huPrP23-144. Relatively rigid residues comprising the amyloid core detected in conventional solid-state NMR experiments are shown in bold black font, with regions having highest β-strand propensity highlighted in grey rectangles (Theint, Nadaud, Surewicz, *et al.*, 2017), and conformationally flexible residues (Helmus *et al.*, 2008, 2010) are shown in grey font. The rectangles below the amino acid sequence schematically show the key huPrP23-144 large deletion variants that were investigated in this study, with the colors of the rectangles corresponding to the colors of the contours in the solid-state NMR spectra in panels (b)-(g). (b-g) 2D  $^{15}$ N- $^{13}$ Cα chemical shift correlation solid-state NMR spectra of  $\Delta$ 28-50 (b, cyan),  $\Delta$ 51-91 (c, gold),  $\Delta$ 28-91 (d, red),  $\Delta$ 92-98 (e, magenta),  $\Delta$ 92-106 (f, green) huPrP23-144 fibrils and  $\Delta$ 92-106 fibrils seeded with WT huPrP23-144 amyloid (g, green), overlaid with the reference spectrum for WT huPrP23-144 fibrils (blue).

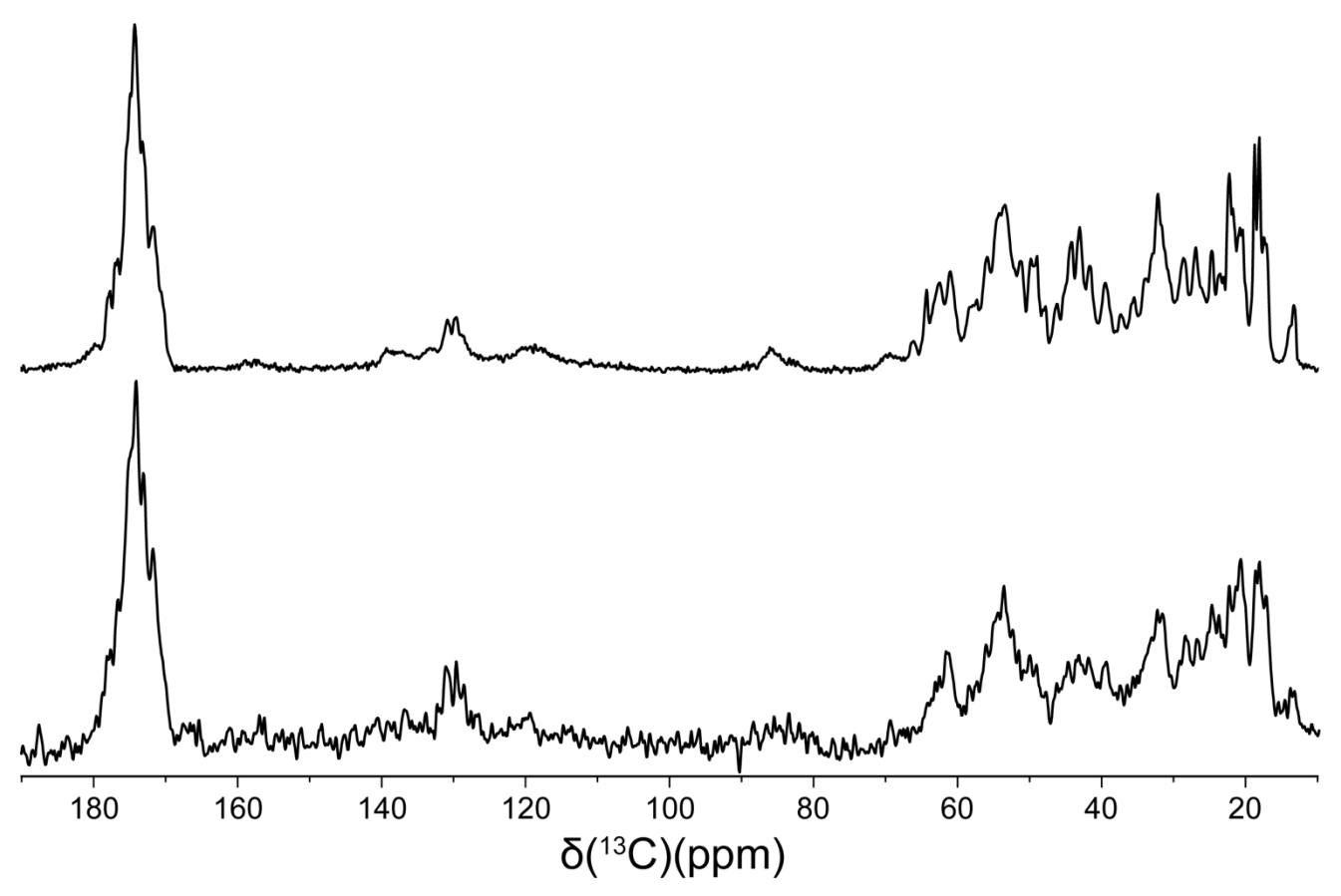


**Figure 4.**  $^{13}$ C CP-MAS spectra of  $^{13}$ C, $^{15}$ N WT (top) and natural abundance  $\Delta 28$ -98 (bottom) huPrP23-144 amyloid fibrils.